2

Biological Signals Identification by a Dynamic Recurrent Neural Network: from Oculomotor Neural Integrator to Complex Human Movements and Locomotion

Guy CHERON[a,b], Françoise LEURS[a], Ana BENGOETXEA[a], Ana Maria CEBOLLA[a], Jean-Philippe DRAYE[a], Pablo D'ALCANTARA[a] and Bernard DAN[a,c]

[a]*Laboratory of Neurophysiology and Movement Biomechanics,*
[b]*Laboratory of Electrophysiology, Université de Mons-Hainaut,*
[c]*Department of Neurology, Hopital Universitaire des Enfants reine Fabiola,*
Université Libre de Bruxelles,
Belgium

1. Introduction

The recent advances in the application of artificial neural networks in the biological field have been inspired by the functional organization of real biological structures (Draye et al.,1997a; Anastasio & Gad, 2007). The fascination exerted by the oculomotor system upon both engineers and neuroscientists have played an important role in this issue. In particular, since the definitive evidence of the existence of a neural integrator in the brainstem (Cheron et al., 1986a; Cannon & Robinson, 1987; Robinson, 1989 for a review) performing mathematical integration of the eye velocity into eye position signals, numerous artificial networks have been developed allowing a better understanding of the fundamental question of how the brain control movement. Such bio-mimetic strategy has recently permitted to elaborate different dynamic recurrent neural networks (DRNN) specifically dedicated to the command of humanoid robot (Tani et al., 2008). Hierarchical neural-inspired modules have also been proposed forming cascades of forward dynamics models (Jordan & Rumelhart, 1992; Kawato et al., 1987; Tani, 2003) in which top-down and bottom-up influences allowed generating behavioural primitives. This Chapter describes the main steps performed in the development of our DRNN from the neural integrator models to those applied in the field of human movement control.

2. DRNN simulation of the oculomotor neural integrator

The interest for neural integrator models outpaces the oculomotor field because the processes involved in the maintenance of eye position presents an analogy with the information held in short-term or working memory (Aksay et al., 2001, 2003; McCormick et al., 2003). When the neuron of the neural integrator persistently discharge for encoding the

Source: Recurrent Neural Networks, Book edited by: Xiaolin Hu and P. Balasubramaniam, ISBN 978-953-7619-08-4, pp. 400, September 2008, I-Tech, Vienna, Austria

time-integral of the eye velocity signals during the saccade, this tonic activity may be interpreted as an internal memory of the eye position in space (Godaux & Cheron, 1996; Chan & Galiana, 2005). The analogy with working memory was thus easily accomplished (McCormick, 2001).

The first neural network approach of the neural integrator was made by Cannon et al. (1983, 1985). Their hard-wired model in which the synaptic weights were explicitly specified can integrate a push-pull input signal without integrating the background rates and has the appealing property that localized artificial lesions produced a decrease in the time constant of the whole network. Later, Anastasio & Robinson (1991) proposed the first learning model for the neural integrator. In this context, we have upgraded the Anastasio-Robinson model in order to work in the continuous-time domain (in opposition to the discrete-time domain). Additionally, we improved the biologically plausible features by (1) the introduction of a strong constraint on the synaptic weight and (2) the introduction of an artificial distance between the neurons by generating delays proportional to the proximity.

2.1 The basic DRNN models

The basic model is a dynamic recurrent neural network governed by the following equations:

$$T_i \frac{dy_i}{dt} = -y_i + F(x_i) + I_i \tag{1}$$

where $F(\alpha)$ is the squashing function $F(\alpha) = (1+e^{-a})^{-1}$, y_i is the state or activation level of unit i, It is an external input (or bias), and x_i is given by:

$$x_i = \sum_j w_{ij}\, y_j \tag{2}$$

which is the propagation equation of the network (x_i is called the total or effective input of the neuron, W_{ij} is the synaptic weight between units i and j). The time constants T_i will act like a relaxation process. The correction of the time constants will be included in the learning process in order to increase the dynamical features of the model. Introduction of T_i allows more complex frequential behaviour, improves the non-linearity effect of the sigmoid function and the memory effect of time delays (Draye et al., 1996; 1997a).

2.2 Fixed-sign connection weights

Traditionally, artificial network represent the synaptic weight by a real number. This number is modified by the learning process (often a gradient-descent kind of minimization) which frequently leads to a sign change at different location. This sign change is in conflict with biological reality and Dale's Principle. Thus we fixed the sign of all connections by the introduction of a variable s_{ij} associated with every weight unit w_{ij}. The variable s_{ij} take their value in the set {-1,0,+1}, and in the classical network propagation equation (2), the weights w_{ij} are replaced by the equation:

$$s_{ij} . \left| w_{ij} \right| \tag{3}$$

The architecture of the network is consistent with the neuroanatomy of the brainstem circuitry of the neural integrator devoted to saccade and vestibulo-ocular systems for the horizontal movements. The figure 1 illustrates the neural integrator DRNN comprising a fully connected hidden layer of 16 inhibitory units, two output units representing the motoneurons of the median and lateral rectus muscle of the left eye and two afferents inputs from the horizontal canal (for the vestibulo-ocular reflex) or from the eye-velocity saccade generator.

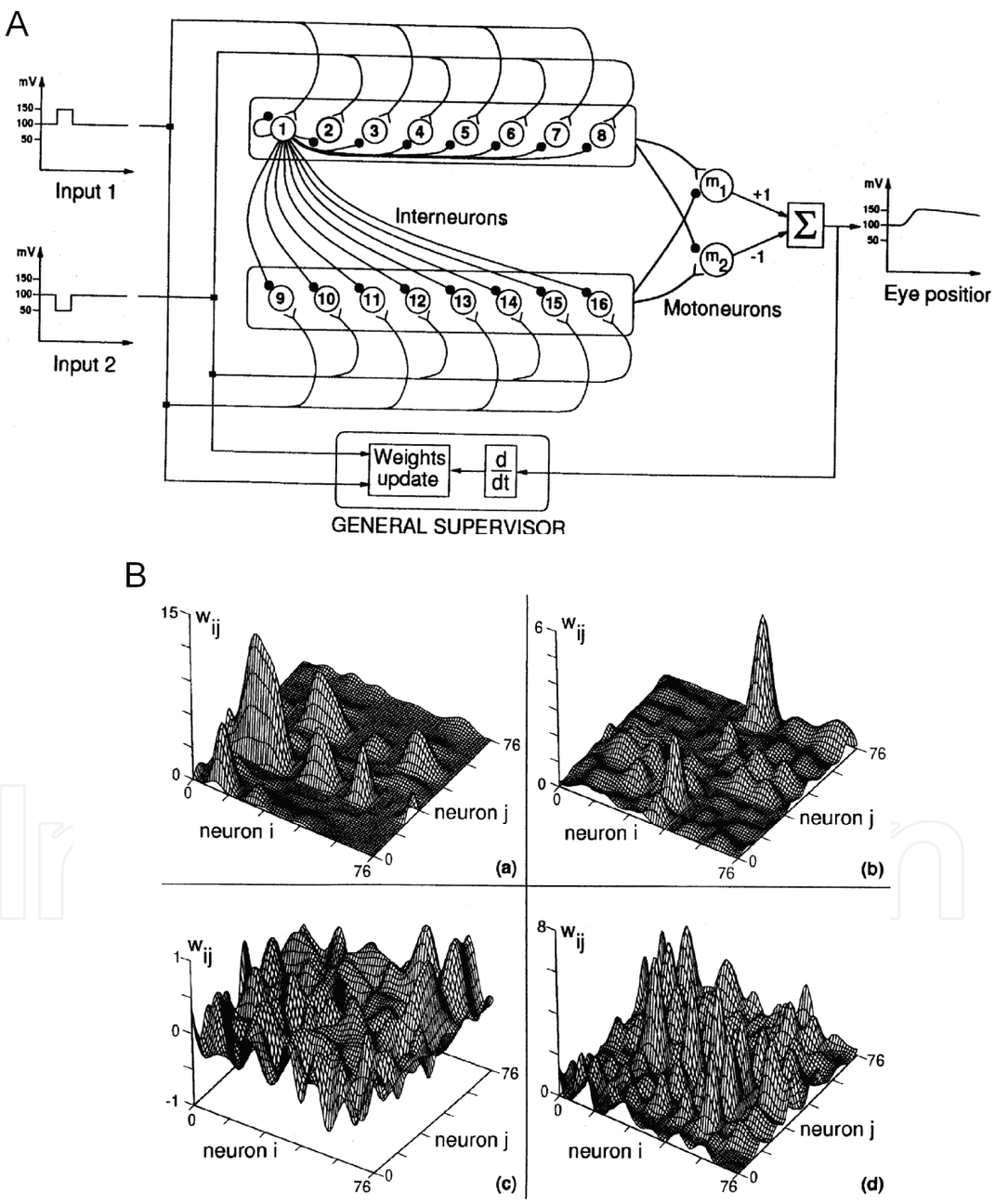

Figure 1. Architecture of the DRNN dedicated to the neural integrator. (A) The 16 interneurons of the hidden layer are divided into two groups of 8 and are fully connected

with inhibitory connections (only the connections from interneuron 1 are depicted). Each interneuron is connected to both motoneurons (output of the network) with a connection whose sign is indicated in the figure. The signals inputs are represented by pulses representing eye-velocity commands of opposite signs. (B) 3D surface plots of the weights distribution. The 16 X 16 weights surface were treated with cubic splines for better visualization. Values of the weights are plotted versus indexes *i* and *j*. Even if the lateral layer has inhibitory connections (except for **c**), the weights are plotted as positives values. **a**, **b** Two clustered structures of the weights distribution. **c**, The weights distribution of the Arnold-Robinson network trained with the general supervisor without any constraints on the weight signs. **d,** The weights distribution in which each interneuron has its own muscle. (*modified from Draye et al. 1997a Biol Cybern)*

2.3 Artificial distance between neurons

Classically, the distances between an artificial neuron labelled 6 and two other neurons labelled 7 and 16 are the same. In order to introduce a real notion of distance in our device (between digits that are memorized in computer memory) we generate delays between these units. The delay between neurons N_i and N_j is defined in order to keep the proportionality to the difference of index $|i-j|$. By this way, the information is *artificially delayed* during its propagation in the network. It will take $|i-j|$ time steps for the information from neuron N_i to reach the neuron N_j.

2.4 Numerical discretization of the continuous-time model

The discrete-time model with a step Δt was defined as:

$$y_i(t+\Delta t) = (1-\frac{\Delta t}{T}) \cdot y_i(t) + \frac{\Delta t}{T} \cdot F(x_i(t)) \tag{4}$$

where

$$x_i(t+\Delta t) = \sum_j w_{ij} \cdot y_j(t) \tag{5}$$

where we assume that the terms $I_i(t)$[see (1)] has been replaced by adaptative weights w_{0i} connected to a fixed input which is set to 1. The discretized equation (5) becomes:

$$x_i(t+\Delta t) = \sum_j \underbrace{(s_{ji} \cdot |w_{ji}|)}_{Fixedsign} \cdot y_j \underbrace{[t-|i-j| \cdot \Delta t^*]}_{Artificialdis\tan ce} \tag{6}$$

For the learning we introduced a *general supervisor* responsible for the modifications of the network weights w_{ij}. In this particular case of the oculomotor integrator simulation, the sign of the connections must be take into account and strictly conserved. This general supervisor continuously computes the amount of the positional deviation (corresponding to the retinal slip) and uses it as an error signal to minimize. The Levenberg-Marquardt minimization technique has been used. The training of the network was done with pulse signals of 50 ms

of duration. After this phase the network produces a position signal compatible with the physiological behavior of the oculomotor neural integrator presenting a time constant of 20s.

2.5 Emergence of clusters

The DRNN was trained a great number of times and each time a clustered structure of the type illustrated in the 3D weights distribution map has emerged (Fig. 1B). A cluster is a region of large weights between a particular group of neurons of index *i* centred on i^* and another group of neurons *j* centred on j^*, where the point $[i^*, j^*]$ is considered as the "centre" of the cluster. The interpretation of a cluster is the following: if the connection weight w_{ij} between two hidden units N_i and N_j is high, *the probability* is high that the connection weight $w_{j(i+1)}$ between one of the neighbours of the source neuron N_{i+1} and N_j is *large. T*he same conclusion can be made for the weight $w_{(j+i)I}$ between N_i and one of the neighbours of the destination neuron N_{j+1}. The mathematical description of the cluster was developed in Draye et al., 1997a. The process of emergence of such clusters during the training phase remains unknown. However, we have studied the conditions for this emergence. Clusters appeared when (1) the sign of the connections was fixed, (2) a lateral inhibitory layer of interneurons, (3) the introduction of an artificial distance between these units and (4) a convergence of information from the hidden layer to the motoneurons. Indeed, when there are no constraints on the weights sign and no delay between the units, there is no clustering structure in the weight distribution (Fig. 1B,c). When we suppressed the convergence of the hidden units on the 2 motoneurons (each interneuron was in this case linked to a muscle), organization in clusters did not appeared anymore (Fig. 1B,d). As we have found that the behaviour (represented by their phase value when sinusoidal input were used) of the units participating to a same cluster was the same (e.g. units presenting eye position sensitivity) (Draye et al., 1997a), an interesting analogy between the artificial DRNN integrator and the electrophysiological recordings can be made. For example, clusters of position neurons have been found in the neural integrator of the cat (Delgado-Garcia et al., 1989; Escudero et al., 1992, 1996; Godaux & Cheron, 1996). We can thus conclude that emergence of clusters in a DRNN performing a well-defined mathematical task (here a temporal integration) is due to computational constraints with a restricted space of solutions. This also suggests that information processing constraints could be a plausible factor inducing the emergence of iterated patterns in biological neural networks.

3. The DRNN application in the field of human movement control

3.1 Introduction

In human, the electromyographic activity (EMG) is the only non-invasively accessible signal directly related to the final command of movement. EMG signal, though not ideal, is a reasonable reflection of the firing rate of a motoneuronal pool (Soechting & Flanders, 1997), and the analysis of rectified EMG envelopes of multiple muscles may reveal the basic motor coordination dynamics (Scholz & Kelso, 1990; Cheron et al., 1996; Bengoetxea et al., 2008).

Our DRNN approach has been firstly applied to the problem of identification of the relationship between EMG signals of the shoulder muscles and the corresponding kinematics of the arm. This identification task is quite complex because the state variables of the system are unknown and identification has to be carried out using only input–output

data. Moreover, the EMG–motion relationship identification task is highly nonlinear. This latter fact complicates the task because it is well known that even in the linear case where the state variables are unknown, a unique parameterization of the system no longer exists (Kalman et al., 1969). The success of nonlinear identification techniques therefore strongly depends upon specific parameterizations used (Wang, 1993).

3.2 Methodological adaptations

The network defined by (1) can be trained using different learning algorithms; the learning algorithm tunes the free parameters to minimize an error measure which is computed as the temporal integration between the real curve and the learned curve. The most famous ones are the real-time recurrent learning algorithm presented by Williams & Zipser (1989) and the time-dependent recurrent backpropagation algorithm derived by Pearlmutter (1989, 1995). The reader can find more details about the learning algorithm in Pearlmutter (1995), Draye et al. (1996, 1997a,c).

In order to make the temporal behaviour of the network explicit, an error function is defined as:

$$E = \int_{t_0}^{t_1} q(\mathbf{y}(t),t)\, dt \tag{7}$$

where t_0 and t_1 give the time interval during which the correction process occurs. The function $q(y(t), t)$ is the cost function at time t which depends on the vector of the neurone activations y and on time. We then introduce new variables p_i (called adjoint variables) that will be determined by the following system of differential equations:

$$\frac{dp_i}{dt} = \frac{1}{T_i} p_i - e_i - \sum_j \frac{1}{T_i} w_{ij} F'(x_j)\, p_j \tag{8}$$

with boundary conditions $p_i(t_1)=0$. After the introduction of these new variables, we can derive the learning equations:

$$\frac{\delta E}{\delta w_{ij}} = \frac{1}{T_i} \int_{t_0}^{t_1} y_i F'(x_j)\, p_j\, dt \tag{9}$$

$$\frac{\delta E}{\delta T_i} = \frac{1}{T_i} \int_{t_0}^{t_1} p_i \frac{dy_i}{dt} \tag{10}$$

The training is supervised; involving learning rule adaptations of synaptic weights and time constant of each unit (see for more details, Draye et al., 1996). Due to the integration of the system of (8) backward through time, this algorithm is sometimes called 'backpropagation through time'. In order to reduce the time of the learning process, the acceleration method of Silva & Almeida, (1990) was used, where each weight and time constant has its own adaptative learning rate.

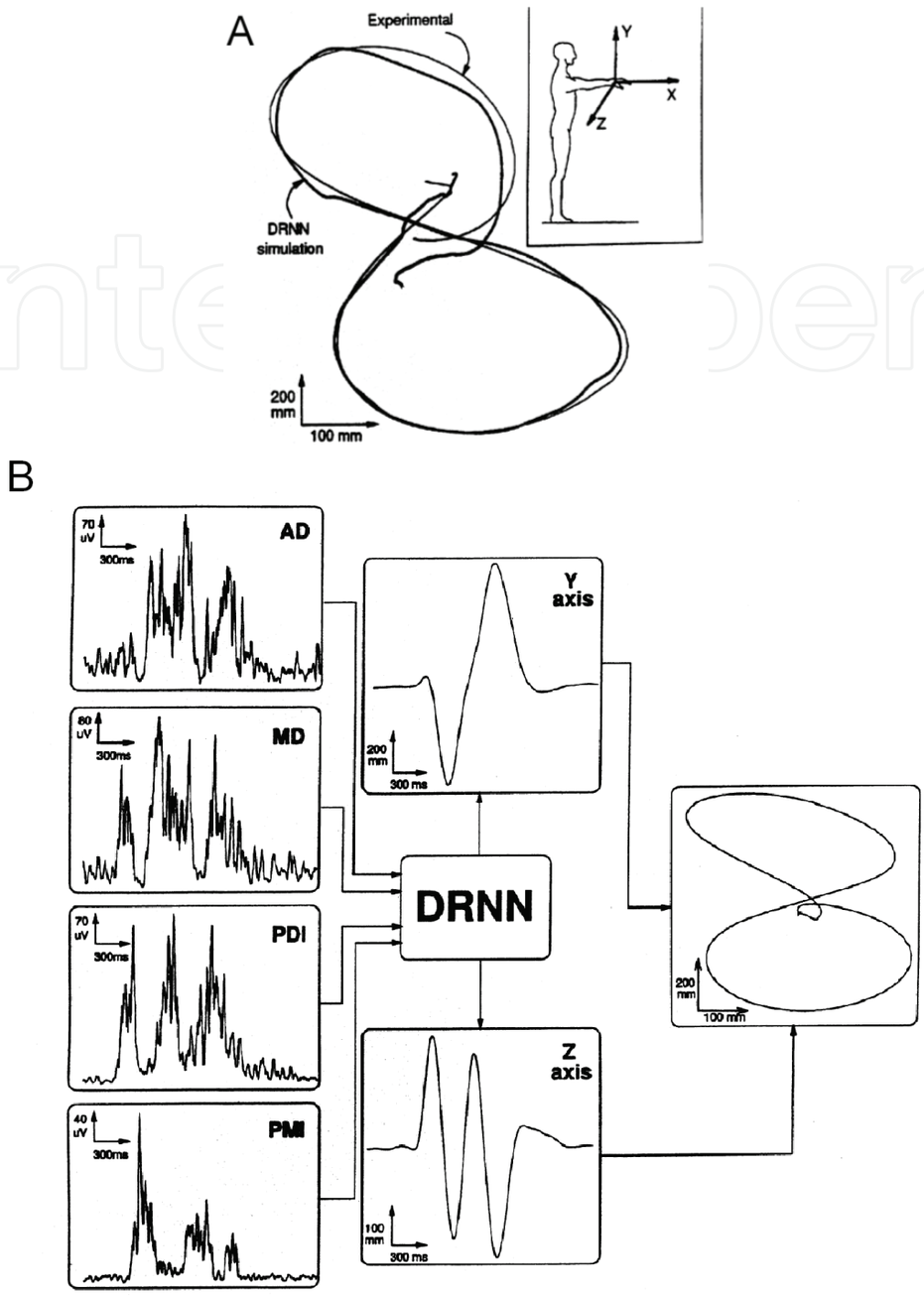

Figure 2. Input-output organization of the DRNN. In this configuration the inputs consist of seven full-wave rectified EMG signals (four of them are depicted). The outputs are the Y and Z coordinates of the index marker during the drawing of the figure eight. The position of the subject and the reference axis are shown on the upper right side. This figurative movement is characterized by two main components in the vertical direction (Y axis-down and up) and by four main components in the horizontal direction (Z axis-right, left, right, and left). In the upper-right inset, superimposition of the experimental trajectory recorded by the ELITE system (thin line) and the simulated curve generated by the DRNN (thick lines). (*Adapted from Cheron et al., 1996 IEEE*)

3.3 EMG and movements recordings

In all experimental situations explored by our group, the DRNN was trained to reproduce the movement performed by the subject in response to the EMG signals as depicted in Fig. 2. In a first set of studies (Cheron et al., 1996; Draye et al., 2002; Bengoetxea et al., 2005), the subjects were asked to draw as fast as possible figures 'eight' with the right extended arm in free space (the initial directions of the movements were up–right, up–left, down–left, and down–right, in that order). We have to note that in this case the kinematics data are given by the position signals of the index finger (the outputs of the DRNN were the vertical and the horizontal position of the index).

In a second set of studies (Cheron et al., 2007) the subjects were asked to perform 'as fast as possible' flexion movements of the elbow in the vertical plane. In this case the angular acceleration of the elbow was used as the output. In the third set of experiments the subjects locomotion was recorded (Cheron et al., 2003; Leurs et al., 2005) and the DRNN presented 3 different output signals corresponding to the kinematics (elevation angle) of the thigh, shank and foot.

These different movements were recorded and analyzed using the optoelectronic ELITE system including two to six TV cameras working at a sampling rate of 100 Hz (BTS, Milano, Italy). Surface EMG patterns were recorded using pairs of silver–silver-chloride surface electrode and measured using telemetry. Raw EMG signals (differential detection) were amplified (1000 times) and band-pass filtered (10–2000 Hz). After this, the EMGs were digitized at 2 kHz, full-wave rectified and smoothed by means of a third-order averaging filter with a time constant of 20 ms. The following muscles were recorded during the figure-eight movement and the elbow flexion: posterior deltoid external and internal (PDE and PDI), anterior deltoid (AD), median deltoid (MD), pectoralis major superior and inferior (PMS and PMI), latissimus dorsi (LD), biceps and triceps brachii. For the locomotion: rectus femoris (RF), vastus lateralis (VL), biceps femoris (BF), tibialis anterior (TA), gastrocnemius lateral (GL), soleus (SOL). The basic mapping between EMG signals input and kinematics output is illustrated in the figure 2 during the execution of the figure eight movement. The superimposition of the real (experimental) and simulated movement well illustrated the DRNN performance.

3.4 From DRNN performance to biological plausibility

For each type of the movement studied, the DRNN has successfully learned the task and was able to reproduce correct output signals with the same type of unlearned EMG signals as input. The learning performance was firstly examined on-line by inspection of the error curve as those illustrated in the case of walking movement (Fig. 3A) (Cheron et al., 2003). Successful learning was commonly ascertained on the basis of the comparison between the DRNN output and the actual output (provided by experimental data). Figure 3 illustrates the superimposition of these data (Fig. 3B-D) when the training has reached an error value of 0.001. The learning process (performed in this case by means of 35 fully connected units) was carried out for 5000 iterations which takes about 5 min on a Intel Core2 at 2 GHz

In order to test the physiological plausibility of the DRNN identification, the basic idea was to compare the angular directional change induced by artificial EMG suppression or potentiation of a single muscle with the physiological knowledge of the pulling direction of the muscle. This method is illustrated for the figure eight movement where a small artificial lesion was performed on the first burst of the PMI muscle. In this case, the last part of this

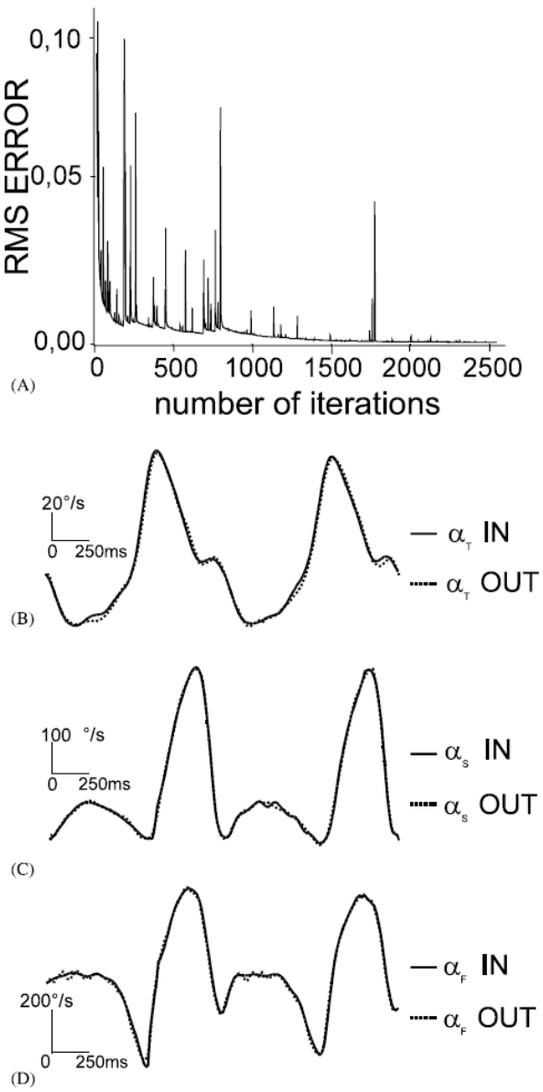

Figure. 3. Assessment of successful learning. (A) Error curve of one learning trial reaching an error value of 0.001 after 5000 iterations. (B, C and D) Superimposition of experimental (continuous line) and DRNN (pointed line) output signals when training reaches an error value of 0.001. (*with permission of Elsevier, Cheron et al. 2003 J Neurosci Meth*)

burst (Fig. 4 a) has been cut off during 50 ms. This altered signal, and the six other unaltered EMG signals are fed to the DRNN previously trained with the normal one. The resulting trajectory is compared to the normal one (Fig. 4 b). This shows that in this case the arm is not able to reach the lower part of the normal trajectory, which is compatible with the physiological action of the PMI acting as extensor-flexor of the shoulder. The quantification of these effects was performed by the computation of the error vector of the arm velocity (Fig. 4 c). For the majority of these lesion experiments performed in the EMG signals of different muscles the direction of the error vector coincided with the preferential field of activation of the corresponding muscle (Cheron et al., 1996). In this context the treatment of the EMG signals by means of different biological filters (Hill-type muscle model) including

tension-length and force-velocity relationships of muscle-tendon actuators can provide a good approximation of muscle force and facilitate the DRNN learning (Draye et al., 1997b). However, contamination of the original neuronal input (raw EMG) by output kinematics-related data (muscle length changes) would bias the spontaneous emergence of multiple attractor states linked to the basic input–output mapping.

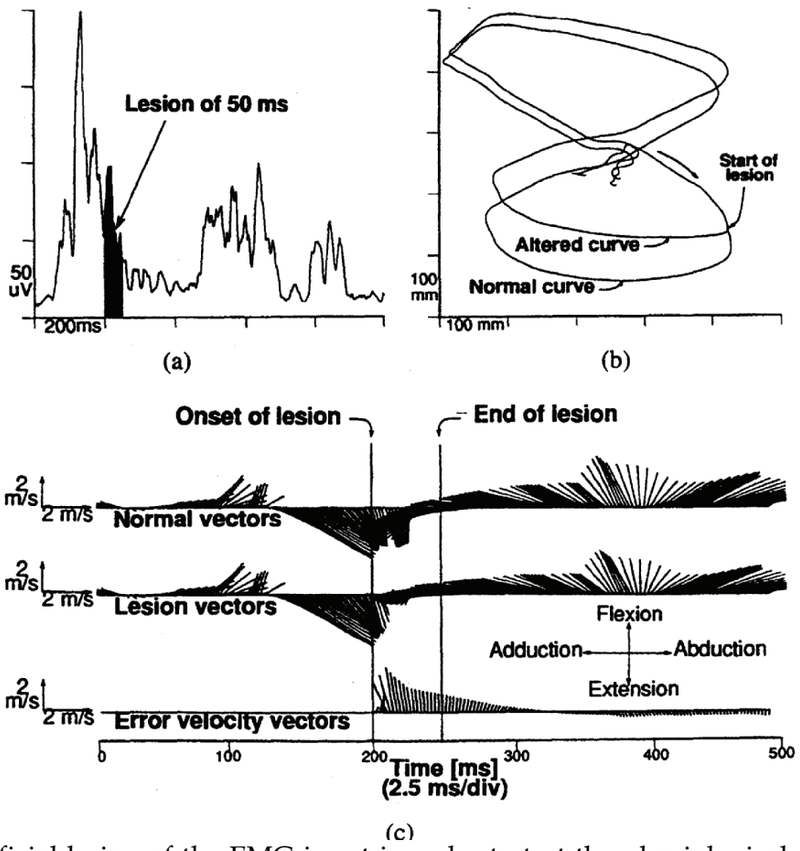

Figure 4. Artificial lesion of the EMG input in order to test the physiological plausibility of the DRNN. (a) Small lesion of 50 ms of duration on the EMG signal recorded on the PMI. (b) Superimposition of the normal and altered trajectories. (c) Velocity vectors of the normal and altered trajectories. The error velocity vectors are obtained by the difference between the preceding ones. (*From Cheron et al.,1996 IEEE*).

The physiological plausibility of our DRNN methods has recently be tested for the identification of the triphasic EMG patterns sub serving the execution of ballistic movements (Cheron & Godaux, 1986b). This pattern comprise a first burst of activity in agonist muscle (AG1) followed by a burst in the antagonist muscle (ANT) and again by second burst in the agonist (AG2). Figure 5 shows that the DRNN is able to perfectly reproduce the acceleration profile of the ballistic movements. The physiological plausibility was tested on all the networks that reached an error level below 0.001 by selectively increasing the amplitude of each burst of the triphasic pattern and evaluating the effects on the simulated accelerating profile. Nineteen percent of these simulations reproduced the physiological action classically attributed to the 3 EMG bursts: AG1 increase showed an increase of the first accelerating pulse, ANT an increase of the braking pulse and AG2 an increase of the

clamping pulse. Another important result was that the DRNN also recognized the physiological function of the time interval between AG1 and ANT, reproducing the linear relationship between this time interval and movement amplitude (Fig. 6). Experimental (Cheron & Godaux, 1986b) and clinical evidence from cerebellar patients (Manto et al., 1995) demonstrated that this time interval is one of the main parameters underlying hypermetria, the other parameter being impaired control of ANT amplitude when inertia is increased.

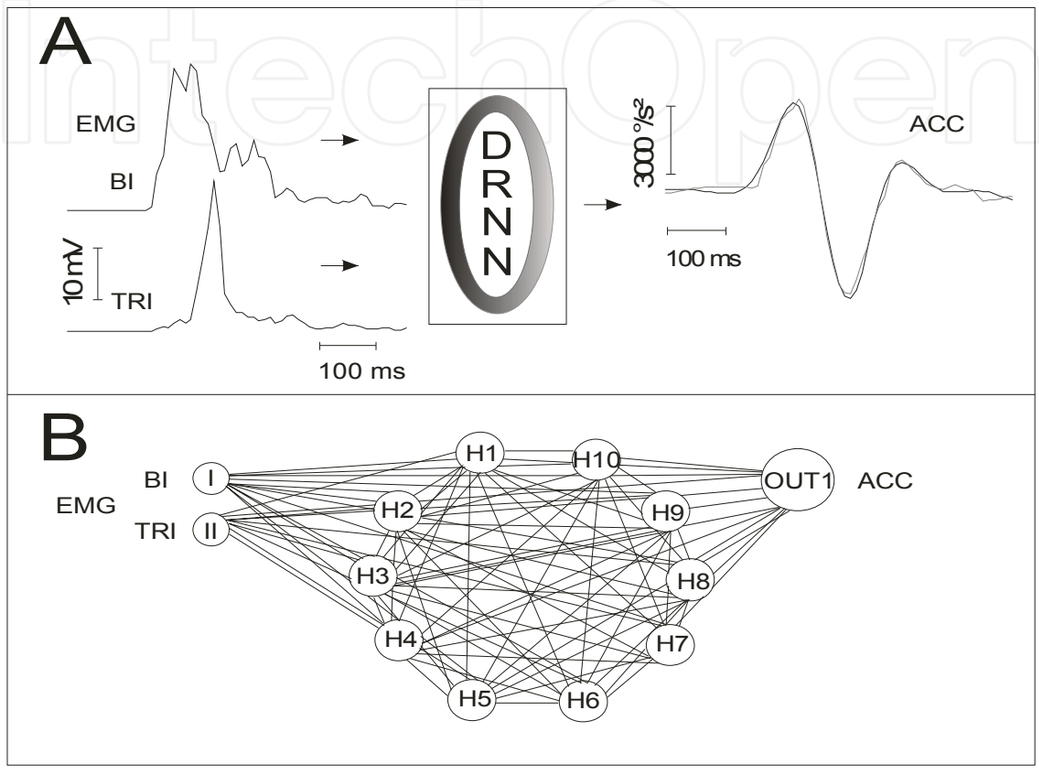

Figure 5. A, Input-output configuration of the DRNN, symbolised by the ring in the central box, with the triphasic EMG pattern as the input and the angular acceleration of the elbow (ACC) used as output. The experimental (grey) and simulated (black) acceleration curves are superimposed. B, DRNN fully connected architecture is represented in case of only 13 artificial neurons (10 hidden neurons, H1-H10; 2 input neurons, I and II, and one output neuron, OUT1).(*Modified from Cheron et al., 2007 Neurosci. Let)*

If the biomechanical knowledge about effect of artificial modifications of the EMG profiles is easily accessible for mono-articular muscles, it is less straightforward for the pluri-articular muscles. In the latter, the muscle force can be involved in a force regulation process for which the directional action is not directly defined by the pulling direction of the muscle. Moreover, dynamical coupling between the three joint segments can be implicated in the evoked movement. For example, in the figure 7 we illustrates the effect of SOL and TA artificial potentiation applied throughout the walking sequence on the sagittal lower limb kinogram over two steps. Whereas the former results in digitigrade gait (explained by the pulling action of SOL) with increased knee flexion (explained by a coupling action) more marked during the swing phase, the latter results in increased ankle dorsiflexion (walking on the heel explained by the pulling action of TA) and knee hyperextension (coupling

action) more marked during the stance phase. The implications of such complex dynamical simulations of biomechanics and muscle coordination in human walking have been recently revisited by Zajac et al. (2003).

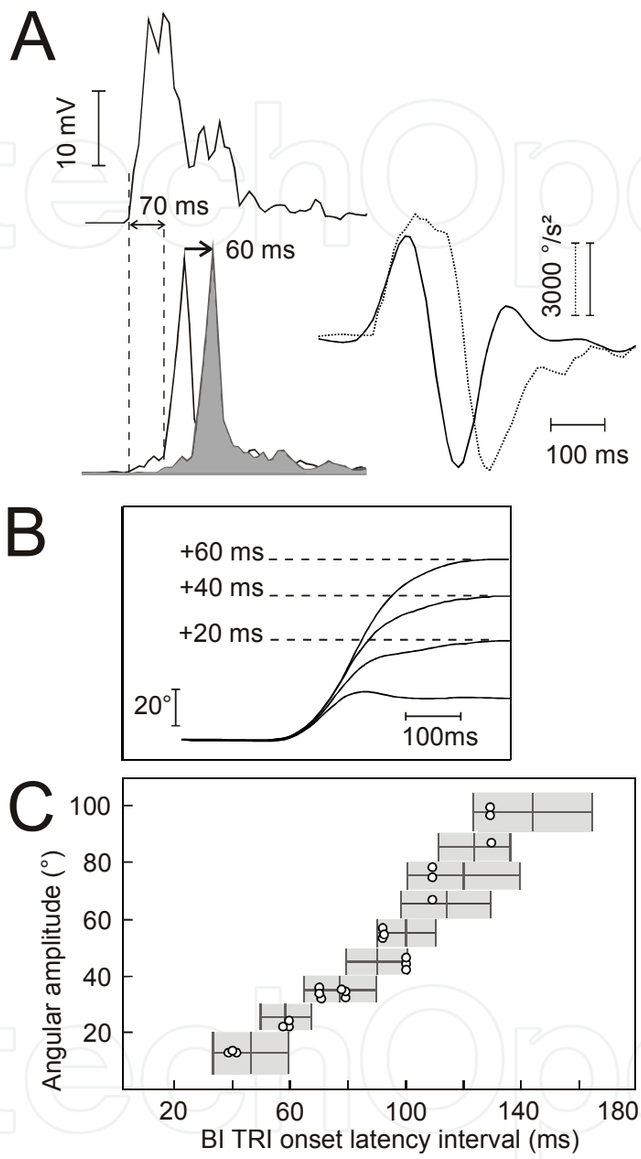

Figure 6. Simulation of AG1-ANT time interval increase on movement amplitude. A, example of a time shift of ANT burst (delayed from 60 ms, grey shading of ANT burst superimposed to the experimental pattern). In the left side, the corresponding ACC curves are superimposed (simulated curve in pointed line and experimental curve in continuous line). B, progressive increase of angular amplitude when the AG1-ANT interval is increased from 20 ms. C, AG1-ANT time interval and the related movement amplitude. Superimposition of the experimental relationship (the mean and SD are represented by the centre and the borders of the grey area, respectively) and the DRNN simulated data (open circles). (*From Cheron et al., 2007 Neurosci. Let)*

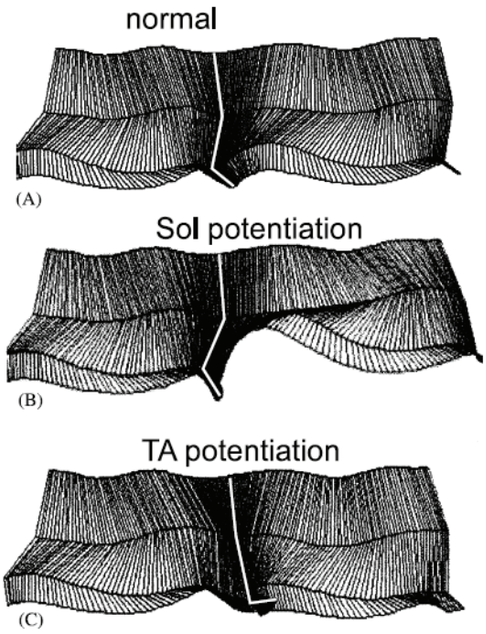

Figure 7. (A–C) Sagittal stick diagrams of the lower limb kinematics obtained after DRNN learning of normal locomotion (A) and after artificial EMG potentiation of SOL (B) and TA (C) muscles. (*From Cheron et al., 2003 J Neurosc Meth, copyright Elsevier*)

4. DRNN with modular architecture

4.1 Introduction of position and inertial subnetworks

We modified the structure of our neural network in order to cope with one of the main drawbacks of trained neural networks: the ''solution'' appears as a black box from which it is difficult to retrieve any information. For this we modified the network architecture in order to include two distinct sets of output neurons: one set related to posture and the other one related to inertia. The postural–output neurons were trained to produce position reference signals, i.e., postural-related data. The inertial–output neurons were trained to produce inertial related data: acceleration signals. The input neurons remain unchanged: they feed the network with the EMG signals. Postural output neurons are fed by 20 fully connected neurons which form a subnetwork that will be called ''the postural subnetwork'' (its neurons are labeled ''1'' to ''20'' in Fig. 2). Similarly, inertial–output neurons are fed by another set of 20 fully connected neurons which form the ''inertial subnetwork'' (its neurons are labeled ''21'' to ''40'' on Fig. 8).

We imposed a communication channel between both ''sub-networks'' This consists of 40 interconnections between corresponding neural units. In other words, the learning algorithm is allowed to adapt the interconnection weights between neurons 1 and 21 (and accordingly between 21 and 1), 2 and 22 (22 and 2), . . ., 19 and 39 (39 and 19), and finally 20 and 40 (40 and 20). These weights are shown as dashed lines in Fig. 8. In this configuration, the entire network has 1172 free parameters (interconnection weights and time constants). The modified architecture as presented above is trained as a single homogeneous network which includes seven input neurons (EMGs) and four output neurons (postural Y and Z, inertial Y and Z). The error evaluation criterion is the same for all four output neurons.

These four identical error signals are used by the TDRBP algorithm to adapt all the free parameters of the network. This type of modular DRNN has been used for the figure eight movement and for the straightening-up movement. The architecture of the network in the latter case is slightly different since the network exhibits eight EMG input signals (versus seven) and three output neurons (versus two). Each subnetwork still consists of 20 neurons. The postural subnetwork generates the angular position signals of the three joints, whereas the inertial subnetwork provides their angular acceleration signals. This network has 1192 free parameters.

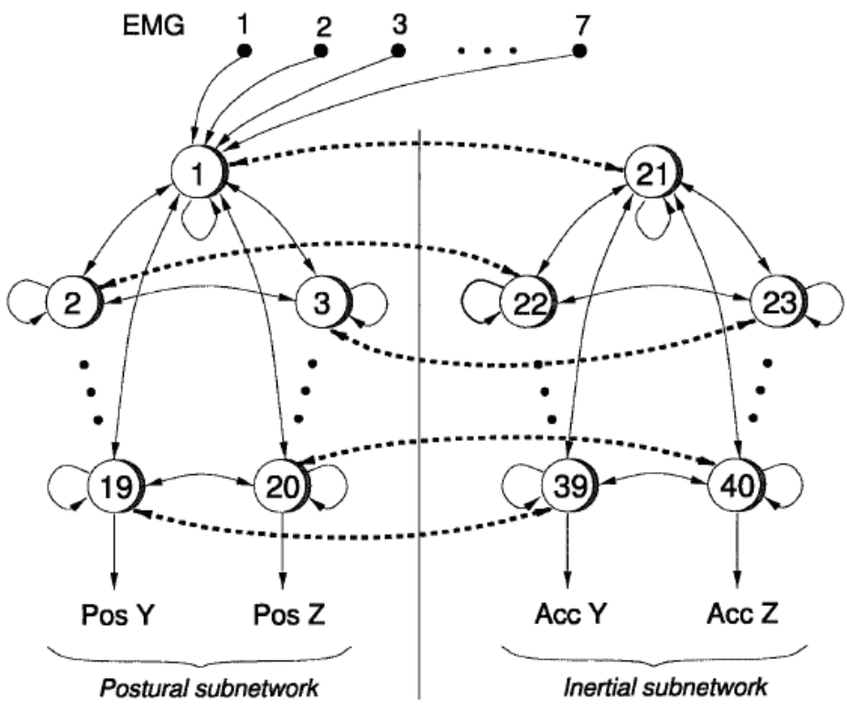

Figure 8. Modular neural architecture with two subnetworks: the first one is related to posture and generates position signals, the second one is related to inertia and generates acceleration signals. The network shows the simulation network for the figure-eight movement case (seven EMG input signals and two kinematics output signals). Note that only some representative connections are depicted (e.g., the input connections are only depicted from input neurons 1 to 7 to neuron 1; the same connections exist between all the input neurons and neurons 2–40). The dashed lines show the interconnections corresponding to the communication channels between both subnetworks. Pos, position; Acc, acceleration. (*From Draye et al., 2002 Biol. Cyber*)

In order to quantify the efficiency of the 40-neuron modular architecture, we compared its performance with the same network without communication channels (in this case, the error signals measured on the postural output signals only affect the postural subnet, and the error signals measured on the inertial output only affect the inertial subnet). We trained this network for 20 times (each new training process started with a new initial random weight distribution). The corresponding error curves were averaged over these 20 learning phases. We have found that the modular network (40-neuron with two communicating subnetworks) gives much better results than the two independent 20 neurons (Fig. 9).

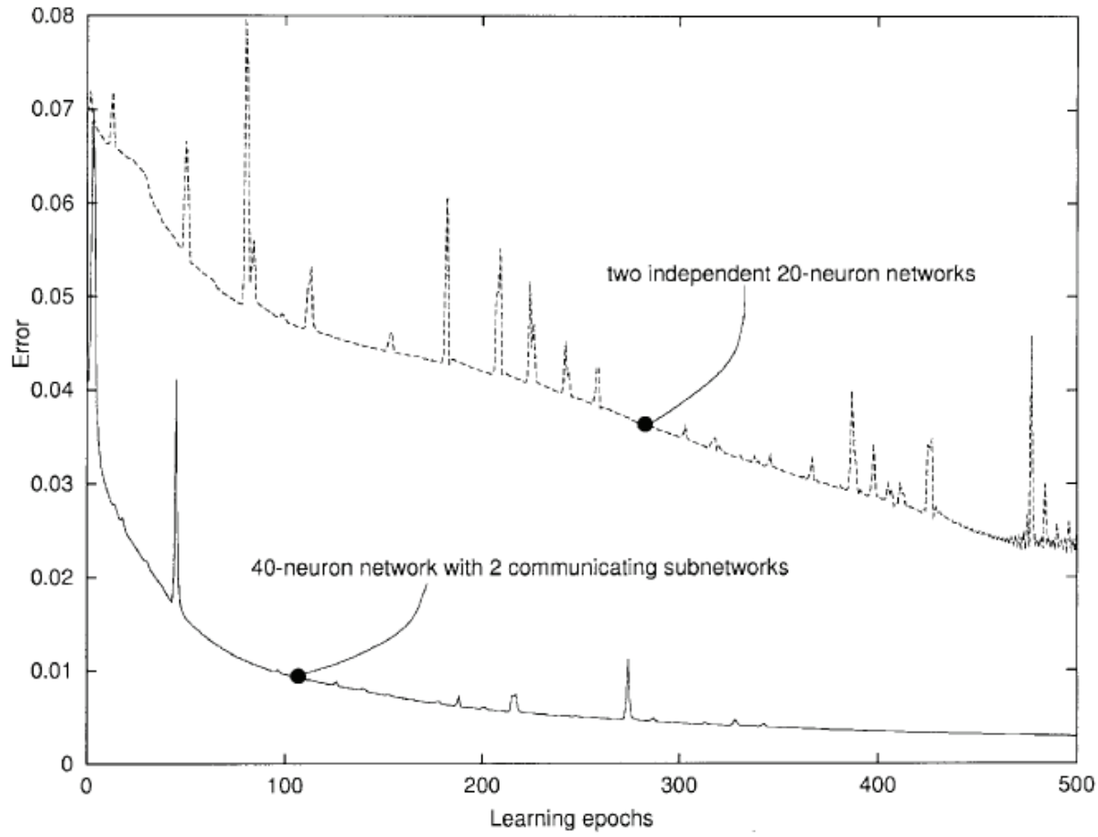

Figure 9. Averaged error curve for the 40-neuron modular architecture (solid line) compared to the cumulative averaged error curves of two independently trained 20-neuron networks (dashed line).

4.2. A Gaussian factor for the artificial distance

In order to improve the biologically plausible features and as previously explained, we decided to introduce a notion of distance in the network using a Gaussian factor aG that modulates all the interconnection weights (from neuron i to j) is replaced by aGw_{ij} where aG is computed using the absolute value of the difference between the indexes i and j (see Draye et al., 2002 for more details). The impact of a particular neuron is greater for neurons with close indexes. We assumed that the hidden neurons were distributed along a circumference; this means that the last hidden neuron (neuron 18) has two nearest neighbors: neurons 17 and 1. Thus, the largest distance between two neurons is 9. In contrast to the artificial distance presented in the simulation of the neural integrator (Draye et al., 1997a) which is based on temporal concepts, the distance presented for the identification of EMGs-movement simulation was based on spatial aspects.

4.2 Emergence of a reduced modular architecture

Following the introduction of an artificial distance a reduced modular architecture has emerged. When only the free parameters that were set to a nonzero value by the learning algorithm have been taken into account, a reduced architecture appeared. It has 524 free parameters (compared with the original configuration of 1172 parameters). Moreover, after

several attempts, we found out that the minimal architecture to solve the first identification task (figure–eight movement) is composed of 20 neurons (two ten-neuron subnetworks). This model includes 244 free parameters. The same network (with eight input neurons and three output units) can solve the second task (standing-up movement); it consists of 274 free parameters. In summary, we showed that with the minimal architecture, the analysis of the network is much easier; there was less redundancy in the network and the number of free parameters has decreased drastically (a factor of about 5!).

4.3 Emergence of inhibitory feedback connections

We have demonstrated that the reduced architecture always exhibited strong feedback inhibitory interconnections between the two sub-network units. The signs of these feedback connection weights have been selected by the learning algorithm. We also noticed that the learning algorithm was more efficient when we initialized the feedback connection weights with negative values prior to the training phase. The emergence of a reduced lateral inhibitory output layer between both subnetworks is consistent with the model proposed by Cannon & Robinson (1983, 1985) to simulate the neural integrator of the human oculomotor system. It is interesting to point out the fact that in our case, the lateral inhibitory connections appeared during the learning process (and was not forced analytically as in Cannon & Robinson (1983, 1985).

4.4 Time-constant and tonic-phasic behaviour of the hidden neurons

The minimal aspect of the reduced DRNN organization allowed studying the distribution of the time constant and the temporal evolutions of the hidden neurons' output. A clear distinction has appeared between the time constants of the position subnetwork units and the inertial subnetwork ones.

This bimodal distribution of the time constants is depicted in Fig. 10 A,B for the figure eight and the straightening-up movement, respectively. These values were averaged over ten different trained networks for each task. The difference between the values of the subnetwork's time constants proves that the individual role of each subnetwork (postural and inertial) has been clearly identified. A higher time-constant mean value in the postural subnetwork is compatible with the task assigned to this subnetwork. In the same line of evidence, we noticed that some the hidden neurons exhibited a phasic behavior (Fig. 10C) while others present a tonic behavior (Fig. 10D). This result is in accordance with the existence of tonic and phasic neurons found in different brain nuclei (such as in the oculomotor system). For example, in the paramedian reticular formation, the eye velocity signal (excitatory or inhibitory burst neurons, Henn et al., 1982) are phasic neurons whereas a group of tonic neurons encode a pure position-related signal in the prepositus hypoglossi nucleus (Escudero & Delgado-Garcia, 1988; Escudero et al., 1992; Godaux & Cheron, 1996). The coding of movement parameters of the premotoneuronal cells recorded in the motor cortex of behaving animals (Fetz et al. 1989) and in the red nucleus revealed that they exhibit at least a pure tonic, a phasic-tonic, or a pure phasic discharge pattern during a ramp-and-hold movement (Fetz, 1992). It is interesting to note that a comparable separation of phasic and tonic drives was obtained by principal component analysis of raw EMG signals (Flanders, 1991). Although, the phasic and tonic EMG patterns are mixed in the raw EMG signals, they might be implemented by distinct neural subnetworks as suggested by Pelligrini

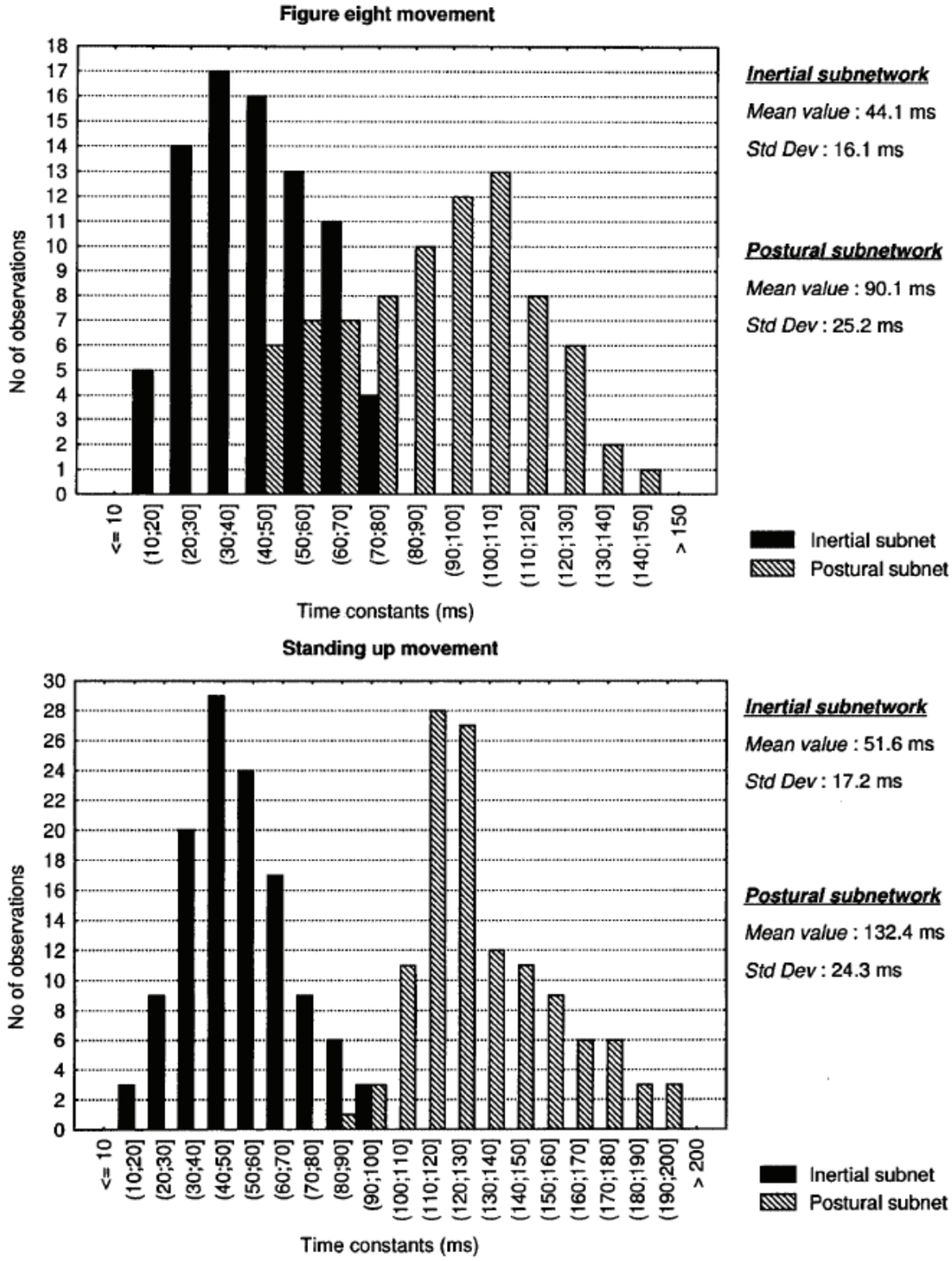
Figure eight movement
No of observations
Time constants (ms)
<= 10
(10;20]
(20;30]
(30;40]
(40;50]
(50;60]
(60;70]
(70;80]
(80;90]
(90;100]
(100;110]
(110;120]
(120;130]
(130;140]
(140;150]
> 150
Inertial subnetwork
Mean value : 44.1 ms
Std Dev : 16.1 ms
Postural subnetwork
Mean value : 90.1 ms
Std Dev : 25.2 ms
Inertial subnet
Postural subnet
Standing up movement
No of observations
Time constants (ms)
<= 10
(10;20]
(20;30]
(30;40]
(40;50]
(50;60]
(60;70]
(70;80]
(80;90]
(90;100]
(100;110]
(110;120]
(120;130]
(130;140]
(140;150]
(150;160]
(160;170]
(170;180]
(180;190]
(190;200]
> 200
Inertial subnetwork
Mean value : 51.6 ms
Std Dev : 17.2 ms
Postural subnetwork
Mean value : 132.4 ms
Std Dev : 24.3 ms
Inertial subnet
Postural subnet

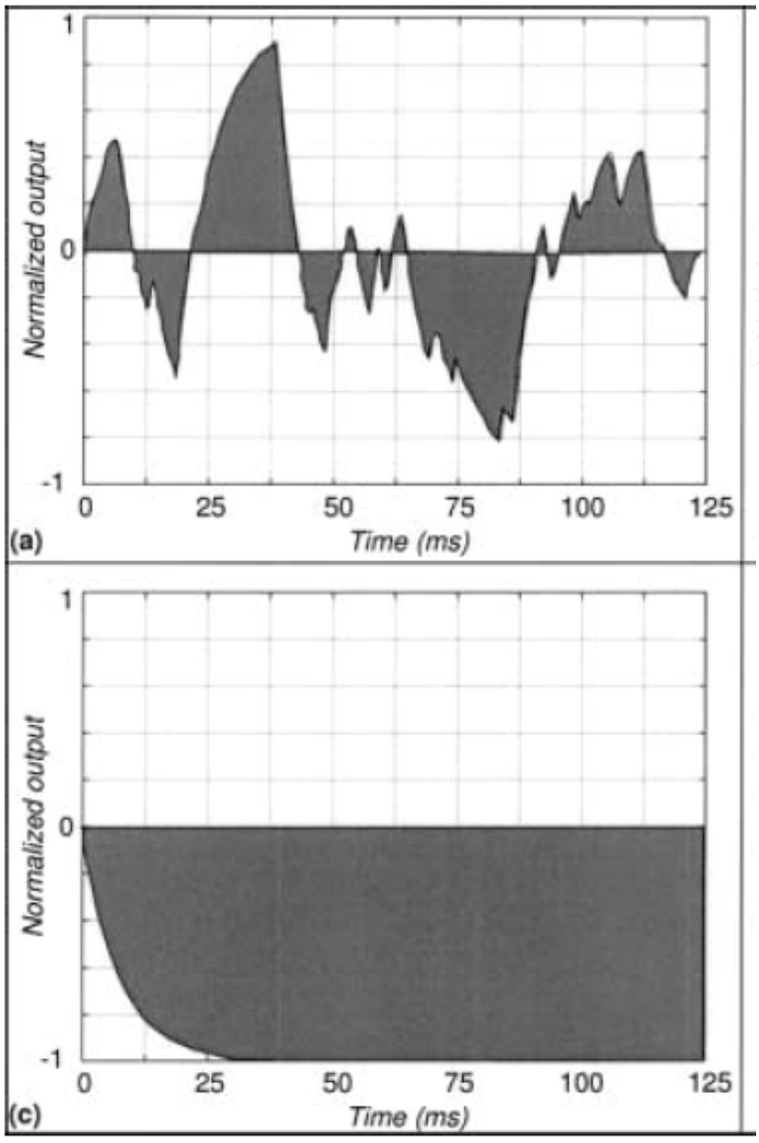

Figure 10. Histograms of the time constants in both postural and inertial subnetworks in the cases of the figure-eight movement (top) and of the standing-up movement (bottom). Temporal evolutions of the hidden neurons output: a,b The output signals of a t phasic hidden neuron and a tonic neuron.

& Flanders (1996). This idea is indirectly confirmed by the present result: The fact that the DRNN mapping between raw EMG signals and the related human movements gives rise to phasic and tonic artificial neuronal substrates is consistent with the neurophysiology of movement control.

In conclusion, the physiological plausibility obtained by our DRNN approach in different aspect of movement control might be of benefit for the potential use of the DRNN in prosthetic control (Craelius, 2002). In particular, the emergence of artificial structures within the DRNN architecture resembling to biological network could be used as a dynamically

adaptive interface between EMG signals from residual muscles and artificial actuators (Cheron et al., 2003). New DRNNs would be dedicated to a larger repertoire of learned movements with generalized properties for the building of a patient-specific dynamical memory of motor actions.

5. References

Aksay, E.; Gamkrelidze, G.; Seung, H.S.; Baker, R. & Tank, D.W. (2001). In vivo intracellular recording and perturbation of persistent activity in a neural integrator. *Nat Neurosci*., 4(2),184-93.

Aksay, E.; Baker, R.; Seung, H.S.& Tank, D.W. (2003). Correlated discharge among cell pairs within the oculomotor horizontal velocity-to-position integrator. *J Neurosci*., 23(34), 10852-8.

Anastasio, T.J. & Robinson, D.A. (1991). Failure of the oculomotor neural integrator from a discrete midline lesion between the abducens nuclei in the monkey. *Neurosci Lett.*, 127(1), 82-6.

Anastasio, T.J. & Gad, Y.P. (2007). Sparse cerebellar innervation can morph the dynamics of a model oculomotor neural integrator. *J Comput Neurosci.*, 22(3), 239-54.

Bengoetxea A, Leurs F, Cebolla A, Wellens S, Draye Jp, Cheron G.(2005) A dynamic recurrent neural network for drawing multi-directional trajectories.*Comput Methods Biomech Biomed Engin.* Supp. 8:29-30.

Bengoetxea, A., Dan, B., Pozzo, T., Gillis, P., Leurs, F. And Cheron, G. (2008) Fast drawing movements: reciprocal muscle patterns encoded in a figure-centered coordinate frame (submitted)

Cannon, S.C.; Robinson, D.A. & Shamma, S. (1983) A proposed neural network for the integrator of the oculomotor system. *Biol Cybern.,* 49, 127–36.

Cannon, S.C. & Robinson, D.A. (1985). An improved neural-network model for the neural integrator of the oculomotor system: more realistic neuron behavior. *Biol Cybern*., 53, 93–108.

Cannon, S.C. & Robinson, D.A. (1987). Loss of the neural integrator of the oculomotor system from brain stem lesions in monkey. *J Neurophysiol*., 57, 1383–409.

Chan, W.W. & Galiana, H.L. (2005). Integrator function in the oculomotor system is dependent on sensory context. *J Neurophysiol*., 93(6), 3709-17.

Cheron, G.; Godaux, E.; Laune, J.M. & Vanderkelen, B. (1986a). Lesions in the cat prepositus complex: Effects on the vestibulo-ocular reflex and saccades. *J Physiol.,* 372, 75–94.

Cheron, G. & Godaux, E. (1986b). Self-terminated fast movement of the forearm in man : amplitude dependence of the triple burst pattern. *J. Biophys. Biom*., 10, 109-17.

Cheron, G.; Draye, J.P.; Bourgeois, M. & Libert, G. (1996) Dynamical neural network identification of electromyography and arm trajectory relationship during complex movements. *IEEE Trans Biomed Eng*., 43, 552–8.

Cheron, G.; Leurs, F.; Bengoetxea, A.; Draye, J.P.; Destree, M. & Dan, B. (2003). A dynamic recurrent neural network for multiple muscles electromyographic mapping to

elevation angles of the lower limb in human locomotion. *J. Neurosci. Methods*., 30, 95-104.

Cheron, G.; Cebolla, A.M.; Bengoetxea, A.; Leurs, F. & Dan. B, (2007). Recognition of the physiological actions of the triphasic EMG pattern by a dynamic recurrent neural network. *Neurosci Lett*., 414(2), 192-6.

Craelius, W. (2002). The bionic man: restoring mobility. *Science*, 295(5557), 1018-21.

Delgado-Garcia, J.M.; Vidal, P.P.; Gomez, C. & Berthoz, A. (1989). A neurophysiological study of prepositus hypoglossi neurons projecting to oculomotor and preoculomotor nuclei in the alert cat. *Neuroscience*, 29(2), 291-307.

Draye, J.P.; Pavisic, D.; Cheron G. & Libert G. (1996). Dynamic recurrent neural networks: a dynamical analysis. *IEEE Transactions on Systems Man, and Cybernetics*., 26, 692-706.

Draye, J.P.; Cheron, G.; Libert, G. & Godaux, E. (1997a) Emergence of clusters in the hidden layer of a dynamic recurrent neural network. *Biol Cybern*., 76, 365–74.

Draye, J.P.; Cheron, G.; Pavisic, D. & Libert, G. (1997b). Improved identification of the human shoulder kinematics with muscle biological filters. *Lecture Note Series in Computer Science*., 1211, 417-28.

Draye J.P.; Pavisic D.; Cheron G. & Libert G. (1997c) An inhibitory weight initialization improves the speed and quality of recurrent neural networks learning. *Neurocomputing,* 16, 207–24.

Draye, J.P.; Winters, J.M.; & Cheron, G. (2002). Self-selected modular recurrent neural networks with postural and inertial subnetworks applied to complex movements. *Biol. Cybern.*, 87, 27-39.

Escudero, M.; de la Cruz, R.R. & Delgado-Garcia, J.M. (1992). A physiological study of vestibular and prepositus hyglossi neurones projecting to the abducens nucleus in the alert cat. *J Physiol.,* 458, 539–60.

Escudero, M.; Cheron, G. & Godaux, E. (1996). Discharge properties of brain stem neurons projecting to the flocculus in the alert cat. II. Prepositus hypoglossal nucleus.*J Neurophysiol*., 76(3), 1775-85.

Escudero, M. & Delgado-Garcia, J.M., (1988). Behaviour of reticular, vestibular and prepositus neurons terminating in the abducens nucleus of the alert cat. *Exp Brain Res*., 71, 218–22.

Fetz, E.E.; Cheney, P.D.; Mewes, K. & Palmer, S. (1989). Control of forelimb activity by populations of corticomotoneuronal and rubromotoneuronal cells. *Prog Brain Res*., 80, 437–49.

Fetz, E.E. (1992). Are movement parameters recognizably coded in the activity of single neurons? *Behav Brain Sci*, 15, 679–90.

Flanders, M. (1991). Temporal patterns of muscle activation for arm movements in the three-dimensional space. *J Neurosci.,* 11, 2680–93.

Godaux, E. & Cheron, G. (1996). The hypothesis of the uniqueness of the oculomotor integrator: direct experimental evidence in the cat. *J. Physiol.,* 492: 517–27.

Henn, V.; Hepp, K. & Buttner-Ennever, J.A. (1982) The primate oculomotor system. II. Premotor system. *Hum Neurobiol*., 1, 87–95.

Jordan, M. I. & Rumelhart, D. E. (1992). Forward models: Supervised learning with a distal teacher. *Cognitive Science*, 16, 307–54.

Kalman, R.E.; Falb, P.L. & Arbib, M.A. (1969). *Topics in mathematical system theory*, McGraw-Hill, New York.

Kawato, M.; Furukawa, K. & Suzuki, R. (1987). A hierarchical neural network model for the control and learning of voluntary movement. *Biol Cybern.*, 57, 169–85.

Leurs, F.; Bengoetxea, A.; Cebolla, A. & Cheron, G. (2005). Reproducibility of the identification process of stump muscle EMG in prosthetic gait by a dynamic recurrent neural network, *Comput. Methods Biomech. Biomed. Engin*. Supp 1, 181.

Manto, M.; Jacquy, J.; Hildebrand, J. & Godaux, E. (1995). Recovery of hypermetria after a cerebellar stroke occurs as a multistage process. *Ann Neurol.*, 38, 437-45.

McCormick, D.A. (2001). Brain calculus: neural integration and persistent activity. *Nat. Neurosci.,* 4(2), 113-4.

McCormick, D.A.; Shu, Y.; Hasenstaub, A.; Sanchez-Vives, M.; Badoual, M. & Bal, T. (2003). Persistent cortical activity: mechanisms of generation and effects on neuronal excitability. *Cereb Cortex.*, 13(11), 1219-31.

Pearlmutter B.A. (1989). Learning state space trajectories in recurrent neural networks. *Neural Comput.*, 1, 263–69.

Pearlmutter B.A. (1995). Gradient calculations for dynamic recurrent neural networks: a survey. *IEEE Trans Neural Netw.,* 6, 1212–28.

Pelligrini, J.J. & Flanders, M. (1996). Force path curvature and conserved features of muscle activation. *Exp Brain Res,* 110, 80–90.

Robinson, D.A. (1989). Integrating with neurons. *Annu Rev Neurosci.,* 12, 33–45.

Scholz J.P. & Kelso J.A. (1990). Intentional switching between patterns of bimanual coordination depends on the intrinsic dynamics of the patterns. *J Mot Behav.,* 22(1), 98-124.

Silva, F.M. & Almeida, L.B. (1990). Speeding up backpropagation, In: *Advanced Neural Computers*, R. Eckmiller, 151-158, Elsevier, Amsterdam.

Soechting, J.F. & Flanders, M. (1997). Evaluating an integrated musculoskeletal model of the human arm. *J Biomech Eng.,* 119, 93– 102.

Tani J. (2003). Learning to generate articulated behaviour through the bottom-up and the top-down interaction processes. *Neural Netw.*, 16(1), 11-23.

Tani, J.; Nishimoto, R.; Namikawa, J. & Ito, M. (2008). Codevelopmental learning between human and humanoid robot using a dynamic neural-network model. *IEEE Trans Syst Man Cybern B Cybern.*, 38(1), 43-59.

Wada, Y. & Kawato, M. (1992). A neural network model for arm trajectory formation using forward and inverse dynamics models. *Neural Netw.,* 6, 919–932.

Wang, L. (1993). Singular value decomposition based space modelling and Kalman filtering techniques. *PhD thesis, Faculté Polytechnique de Mons*, Mons, Belgium.

Williams, R.J. & Zipser, D. (1989). A learning algorithm for continually running fully recurrent neural networks. *Neural Comput.*, 1, 270–80.

Zajac, F.E.; Neptune, R.R. & Kautz, S.A. (2003). Biomechanics and muscle coordination of human walking: part II: lessons from dynamical simulations and clinical implications. *Gait Posture*., 17(1), 1-17.

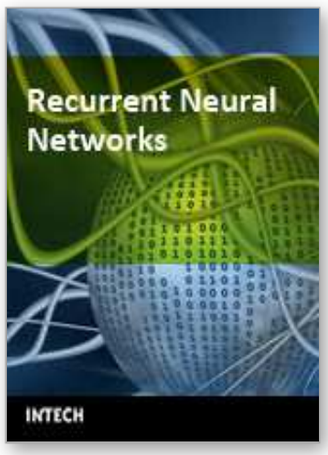

Recurrent Neural Networks

Edited by Xiaolin Hu and P. Balasubramaniam

ISBN 978-953-7619-08-4
Hard cover, 400 pages
Publisher InTech
Published online 01, September, 2008
Published in print edition September, 2008

The concept of neural network originated from neuroscience, and one of its primitive aims is to help us understand the principle of the central nerve system and related behaviors through mathematical modeling. The first part of the book is a collection of three contributions dedicated to this aim. The second part of the book consists of seven chapters, all of which are about system identification and control. The third part of the book is composed of Chapter 11 and Chapter 12, where two interesting RNNs are discussed, respectively.The fourth part of the book comprises four chapters focusing on optimization problems. Doing optimization in a way like the central nerve systems of advanced animals including humans is promising from some viewpoints.

How to reference

In order to correctly reference this scholarly work, feel free to copy and paste the following:

Guy Cheron, Françoise Leurs, Ana Bengoetxea, Ana Maria Cebolla, Jean-Philippe Draye, Pablo D'alcantara and Bernard Dan (2008). Biological Signals Identification by a Dynamic Recurrent Neural Network: from Oculomotor Neural Integrator to Complex Human Movements and Locomotion, Recurrent Neural Networks, Xiaolin Hu and P. Balasubramaniam (Ed.), ISBN: 978-953-7619-08-4, InTech, Available from: http://www.intechopen.com/books/recurrent_neural_networks/biological_signals_identification_by_a_dynamic_recurrent_neural_network__from_oculomotor_neural_inte

INTECH
open science | open minds

InTech Europe
University Campus STeP Ri
Slavka Krautzeka 83/A
51000 Rijeka, Croatia
Phone: +385 (51) 770 447
Fax: +385 (51) 686 166
www.intechopen.com

InTech China
Unit 405, Office Block, Hotel Equatorial Shanghai
No.65, Yan An Road (West), Shanghai, 200040, China
中国上海市延安西路65号上海国际贵都大饭店办公楼405单元
Phone: +86-21-62489820
Fax: +86-21-62489821

IntechOpen